Study on Condensed Matter Simulated by Multiphase Fluid-Solid Coupling Fluid Mechanics

Yingbin Song and Xiaonan Dong

Wuhan Technology and Business University, Wuhan 430065, Hubei, China

Abstract. The hydrodynamic characteristics of a three-phase gas-liquid-solid turbulent bed with light particle flow and intermittent liquid feeding were numerically simulated by CFD program Fluent6.3. The axial and radial motion of particles in a three-phase gas-liquid-solid turbulent bed and the variation of particle concentration in the bed are studied. The results show that the size and frequency of cavitation increase with the increase of the distance from the axis of the air distribution disk and the distance from the bed surface to the central region. The void varied from narrow to wide, while the void changed in the opposite direction. The bubble lift rate and bubble size are basically the same in axial and radial direction. With the increase of the surface gas velocity and the viscosity of the liquid phase, the average particle content in the bed decreases.

Keywords: Gas-liquid-solid; counter current turbulent bed; dynamics; numerical simulation; micro conductivity probe technology.

1. Introduction

The counter current three-phase turbulent bed (ITPTB) is a fluidized bed that can only be reached by rising air flow. Due to its own advantages, it has been used more and more in biochemical reactions in recent years. For example, in biological wastewater treatment, granular particles are used as the carrier of microorganisms, and the gas phase is the only fluidization medium, which is consistent with the characteristics of biological wastewater treatment process requiring high liquid residence time and low liquid velocity. In a three-phase convective turbulent bed, the transfer between gas-liquid and liquid-solid is a large-scale transfer problem [1]. Due to the existence of microparticle support and micro biofilm, the liquid-solid specific surface area is very large, and the mass transfer resistance at the liquid-solid interface is almost negligible. Solids are less dissolved in liquids, so they can be used as research objects for gaseous mass transfer. Although ITPTB has important applications in many fields, the basic physical properties of ITPTB are still very limited. Some scholars have analysed the effects of apparent liquid velocity, apparent gas velocity, initial concentration of solid particles, particle size and density, and type of gas distributor on the flow pattern in the reactor, but did not consider the viscosity of the liquid phase. However, in biochemistry, food and other fields, most of the liquids are highly viscous and non-Newtonian liquids, which restricts the expansion and application of the existing results. So far, there has been no systematic experimental and theoretical analysis of ITPTB in the world. In order to understand the microstructure and dynamic characteristics of ITPTB, this paper provides theoretical basis for the design and scale-up of ITPTB reactors from the microscopic and quantitative perspectives.

2. Experimental analysis

2.1 Experimental equipment

A three-phase reverse fluidized bed test facility is shown in Figure 1 (image cited in the effect of temperature on the distributor design in bubbling fluidized beds). The test was done in a transparent tower made of PMMA. The reactor mainly consists of five parts: gas separation section, liquid distribution section, test section, gas distribution section and liquid separation section [2]. The test section is 1.85 meters high and 0.15 meters wide. The liquid phase flow in the whole tower was realized by introducing the liquid phase from the top of the tower into the tower with 275 liquid phase distribution devices with a diameter of 3.5 mm. The flow meter is used to monitor the flow of gas and

liquid, and the valve is used to control the flow of gas and liquid. Under the influence of vapor-liquid two-phase flow, the solid particles from the top of the tower to the bottom of the tower finally reach a complete fluidized bed.

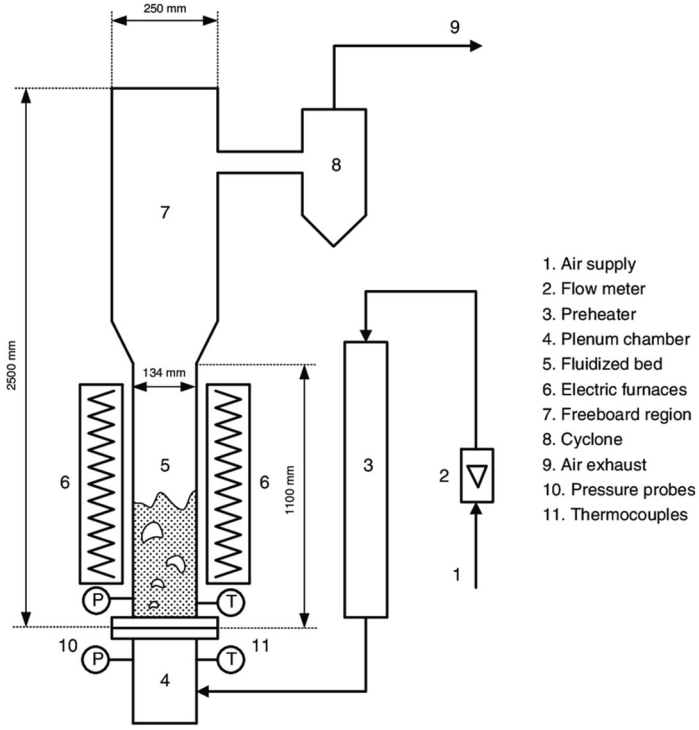

Figure 1. Schematic diagram of the three-phase inverse fluidized bed experimental device

The gas-liquid-solid three-phase inverse fluidized bed was adopted, with defiled compressed air filtered with impurities as the gas phase, water, 0.5% ethanol aqueous solution and sodium carboxymethyl cellulose solution of various concentrations as the liquid phase [3]. The particle size is similar to that used in applications such as sewage treatment, and the concentration of a mixture of alcohol and water is measured. The selected solid phase addition amount should be controlled within 30%.

2.2 Test Process

Kla values were measured by dissolved oxygen electrode kinetics. Dissolved oxygen electrodes are inserted at the top of the reactor to measure the oxygen concentration in the liquid. The instrument for the determination of dissolved oxygen is selected JPB-607, which is produced by Shanghai Lei Magnetic Instrument Company [4]. The detection speed reached tE<1/Kla in less than 30 seconds without correction. The gas is controlled by the pressure, reduced by the pressure relief valve, stabilized by the buffer tank, and then imported by the intake pipe of the reaction unit. First, the three-way valve was fed nitrogen for a period of time, so that the oxygen content of the liquid on the dissolved oxygen instrument was reduced to 0·1 mg·L-1, and the initial oxygen content C0 was measured. The nitrogen is then stopped and the three-way valve is changed to open to air.

2.3 Establishment of numerical model

Mass conservation (continuity) equation:

$$\frac{\partial}{\partial t}(\phi_q \lambda_q) + \nabla(\phi_q \lambda_q d_q) = 0 \tag{1}$$

Gas phase momentum conservation equation:

$$\frac{\partial}{\partial t}(\lambda_g \phi_g d_g) + \nabla(\lambda_g \phi_g d_g d_g) = -\lambda_g \nabla b + \nabla \bar{\bar{\mu}}_g + \lambda_g \phi_g g + \gamma_{ig}(d_i - d_g) \tag{2}$$

The gas phase pressure strain tensor $\bar{\bar{\mu}}_g$ is

$$\bar{\bar{\mu}}_g = \lambda_g \sigma_g (\nabla d_g + {d_g}^T) + \lambda_g (\delta_g - \frac{2}{3}\sigma_g)\nabla d_g \bar{\bar{I}} \tag{3}$$

Momentum conservation equation in liquid phase:

$$\frac{\partial}{\partial t}(\lambda_1 \phi_1 d_1) + \nabla(\lambda_1 \phi_1 d_1 d_1) = -\lambda_1 \nabla b + \nabla \bar{\bar{\mu}}_1 + \lambda_1 \phi_1 g + \gamma_{i1}(d_i - d_1) \tag{4}$$

The liquid phase pressure strain tensor $\bar{\bar{\mu}}_1$ is

$$\bar{\bar{\mu}}_1 = \lambda_1 \sigma_1 (\nabla d_1 + d_1^T) + \lambda_1 (\delta_1 - \frac{2}{3}\sigma_1)\nabla d_1 \bar{\bar{I}} \tag{5}$$

Solid phase momentum conservation equation:

$$\frac{\partial}{\partial t}(\lambda_s \phi_s d_s) + \nabla(\lambda_s \phi_s d_s d_s) = -\lambda \nabla b - \nabla b_s + \nabla \bar{\bar{\mu}}_s + \lambda_s \phi_s g + \gamma_{is}(d_i - d_s) \tag{6}$$

Solid pressure b_s is

$$b_s = \lambda_s \phi_s \Omega_s + 2\phi_s (1 + e_s)\lambda_s^2 g_{0,s} \Omega_s \tag{7}$$

The radial distribution function $g_{0,s}$ is

$$g_{0,s} = [1 - (\frac{\lambda_s}{\lambda_{s,max}})^{\frac{1}{3}}]^{-1} \tag{8}$$

The solid phase pressure strain tensor $\bar{\bar{\mu}}_s$is

$$\bar{\bar{\mu}}_s = \lambda_s \sigma_s (\nabla d_s + d_s^T) + \lambda_s (\delta_s - \frac{2}{3}\sigma_s)\nabla d_s \bar{\bar{I}} \tag{9}$$

The solid shear viscosity σ_s is

$$\sigma_s = \frac{\phi_s \sin \xi}{2\sqrt{I_{2D}}} + \frac{10\phi_s s_s \sqrt{\Omega_s \pi}}{96\lambda_s (1+e_s) g_{0,s}} \left[1 + \frac{4}{5} g_{0,s} \lambda_s (1 + e_s)\right]^2 \tag{10}$$

Solid volume viscosity δ_s is

$$\delta_s = \frac{4}{3}\lambda_s \phi_s s_s g_{0,s}(1 + e_s)\left(\frac{\Omega_s}{\pi}\right)^{1/2} \tag{11}$$

The equations of turbulent kinetic energy κ and dissipation rate ε are respectively

$$\frac{\partial}{\partial t}(\phi\kappa) + \frac{\partial}{\partial x_i}(\phi u_i \kappa) = \frac{\partial}{\partial x_j}\left[\left(\sigma + \frac{\sigma_t}{\sigma_\kappa}\right)\frac{\partial \kappa}{\partial x_j}\right] + G_\kappa - \phi\varepsilon \tag{12}$$

$$\frac{\partial}{\partial t}(\phi\varepsilon) + \frac{\partial}{\partial x_i}(\phi u_i \varepsilon) = \frac{\partial}{\partial x_j}\left[\left(\sigma + \frac{\sigma_t}{\sigma_\varepsilon}\right)\frac{\partial \varepsilon}{\partial x_j}\right] + \frac{\varepsilon}{\kappa}(c_1 G_\kappa - c_2 \phi\varepsilon) \tag{13}$$

Where $\sigma_t = \phi C_\sigma \frac{\kappa^2}{\varepsilon}$

$$G_\kappa = \sigma_t \left[\left(\frac{\partial u}{\partial x} + \frac{\partial d}{\partial y} + \frac{\partial v}{\partial z}\right)^2 + 2\left(\frac{\partial u}{\partial x}\right)^2 + 2\left(\frac{\partial d}{\partial y}\right)^2 + 2\left(\frac{\partial v}{\partial y}\right)^2\right] \tag{14}$$

2.4 Signal acquisition and processing

A microcomputer is used to collect the simulation signals. The length of samples collected each time is 3000, 50 Hz,60 seconds, and the number of bubbles is 50-60, all of which are stored in binary mode [5]. When the bed is fully expanded, the bubbles inside the bed will converge and break, and their frequency, size and rise rate are very random, so the theoretical analysis of them has certain limitations.

3. Test results and discussion

3.1 Effects of apparent gas velocity and solid holdup

Figure 2 shows the effect of the apparent gas velocity of the Kla in the batch test state [6]. With the increase of the apparent gas velocity, the number of bubbles in the solution increases, and the gas holdup of the system significantly increases, thus significantly increasing the Kla. In addition, with the increase of surface air velocity, the average concentration of liquid-solid mixture in the fluidized bed also decreases, which plays a certain role in the retention and mass transfer of foam in the bed.

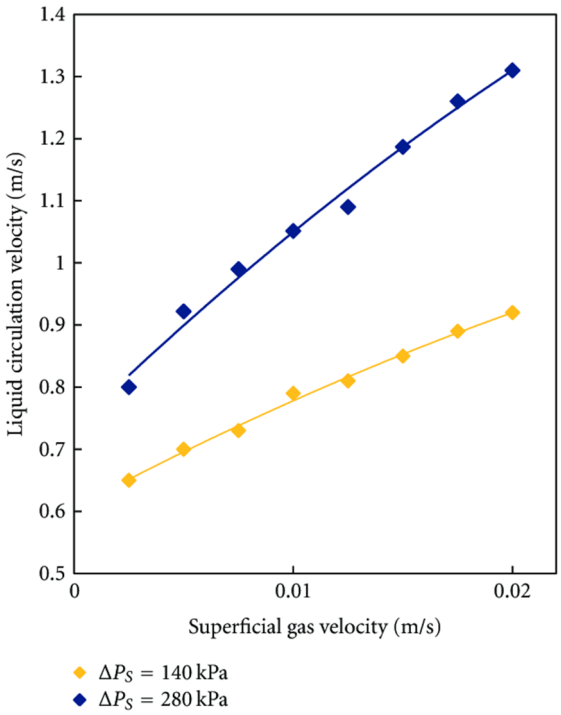

Figure 2. Effect of apparent gas velocity on Kla

Figure 3 is the curve of the change of solid Holdup to Kla. It can be seen from the curve that Kla first increases with the increase of solid holdup. When the solid content is between 0·05 and 0·08, the Kla becomes constant as the solid content increases [7]. The mass transfer characteristics of the three-phase system with different solid-liquid content were investigated on the internal circulation reactor, and it was found that the Kla value reached its peak when the solid-liquid content was about 2%. The results show that the Kla of the liquid phase is the largest at 5% solid phase content.

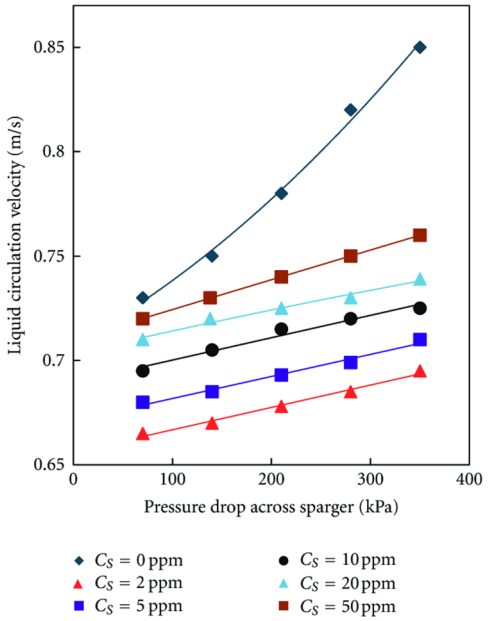

Figure 3. Relationship between solids content and Kla

The Kla of a three-phase system varies with the mass fraction of solid and liquid. 1) The introduction of solid particles will reduce the volume of the gas-liquid phase, reduce the specific surface area of the gas-liquid phase, and then reduce the transfer efficiency of the gas-liquid phase.

2) Due to the addition of solid substances, the apparent viscosity of the fermentation liquid will be significantly increased. When the content of solid material increases, the density and interphase friction of the system will also increase, resulting in the flow resistance of the liquid phase will also increase. At the same time, under the same input quantity, the turbulence of the phase and the dispersion of the gas phase will be weakened, and the fusion of the bubble will be accelerated, and the renewal rate of the gas-liquid interface will be slow, resulting in the reduction of the specific surface area of the gas liquid [8]. These two factors will cause Kla to become lower and lower with the increase of solid content. Moreover, with the increase of solid particle content, its negative effect is also enhanced.

In addition, solid particles also have a positive effect on gas-liquid mass transfer: 1) The distribution of solid particles in the static liquid layer of a single bubble can reduce the surface tension of the bubble, promote the rupture of the bubble, and effectively prevent the polymerization of the bubble. 2) The particles have a certain damage effect on the static liquid film around the bubble, thus shortening the transfer and diffusion distance of the bubble. 3) The tangential force formed by the flow rate difference of gas, liquid and solid trinity in the phase promotes the diffusion of gas and liquid and the rupture of the bubble, and increases the specific surface of the gas and liquid phases. Each element is interactive. In small concentration ranges the positive effects of particles prevail. The anomalous effects of particles dominate in the condition of high solid content. From the point of view of enhanced gas-liquid mass transfer, the optimal solids content is between 0·05 and 0·08, but other parameters need to be combined in the selection of solids content.

3.2 Influence of different factors on bubble rising speed

3.2.1 The apparent gas velocity, the number of solids added and the effect of surface-active substances on the gas velocity.

The apparent gas rate, solids addition, and surface-active substances have different effects on the cavity growth rate (FIG.4 Cited in Processes 2019, 7(12), 936). The results show that different concentrations of solid particles have different effects on the growth rate of cavitation. This is consistent with the law that the foam rise rate is proportional to the foam size in the three-phase fluidized bed.

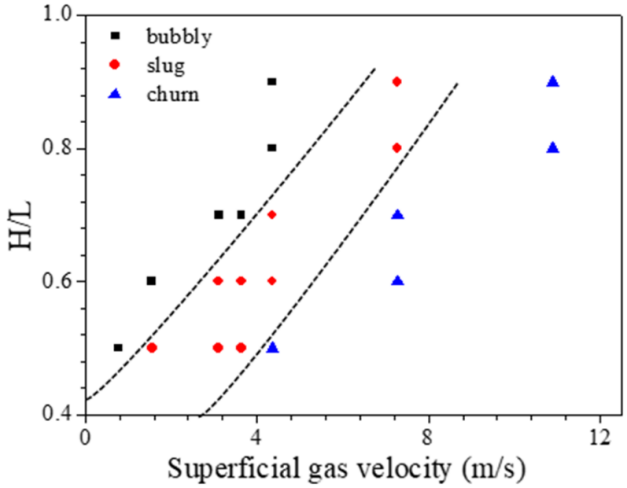

Figure 4. Apparent gas flow rate, solids addition, and the relationship between surfactant and cavity rise rate

3.2.2 Influence of liquid phase velocity, liquid phase viscosity and particle concentration on liquid phase quality.

In FIG. 5, it can be seen that the rise rate of the cavity is affected by the apparent liquid flow rate, liquid viscosity, and particle concentration (image cited in Processes 2019, 7(12), 936). The results show that with the increase of surface flow velocity and fluid viscosity, the surface flow velocity of polyethylene system decreases [9]. The influence of the buoyancy of the upper fluid on the rising

bubble also increases. Moreover, this effect is greater than the viscous drag force, so that the foam rise rate increases with the increase of the viscosity of the fluid. Because the foam rise rate in the three-phase fluidized bed is proportional to the size of the foam, the foam of PP particle system is larger than that of PE particle system.

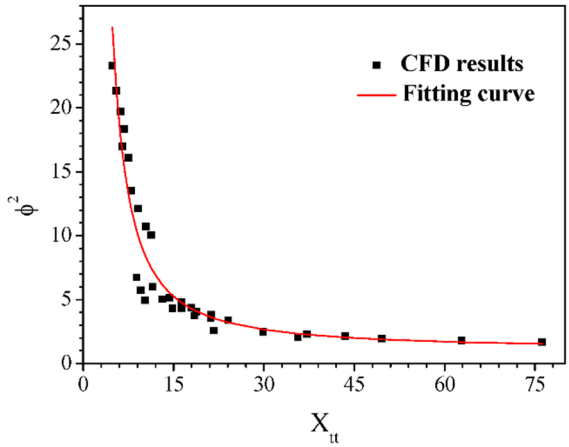

Figure 5. Effects of apparent liquid velocity, liquid viscosity and particle density on bubble rise velocity

4. Conclusion

1) The spread of the bed surface in the reactor is carried out gradually, and there are particle aggregation phenomena before and after particle fluidization. 2) The velocity of particles in the direction of runoff is unbalanced, showing the characteristics of "smaller at both ends and larger in the middle". The radial velocity of the particle is greater than the diameter velocity near the centre of the particle, while the distance near the particle is less than the diameter velocity of the particle.

References

[1] Zhu Miaoyong, Lou Wentao. Numerical simulation of multiphase flow and its reaction dynamics in steelmaking process. Chinese Journal of Materials and Metallurgy, 21(1) (2022)19-23.

[2] Wang Dechen, Zhang Junting, FAN Jiawei. Numerical simulation of bidirectional fluid-structure coupling dynamics of tumor bearing artery. Journal of North University of China: Natural Science Edition, 44(1) (2023)84-88.

[3] Yu Jun, Wang Haikun, Liu Guozhen, et al. Study on the motion characteristics of multiphase flow during underwater near-free surface explosion. Ship Mechanics, 27(2) (2023)103-108.

[4] Ma Kun, He Qiaolin. Simulation of fluid-structure coupling problem based on lattice Boltzmann method. Journal of Sichuan Normal University: Natural Science Edition, 46(2) (2021)72-77.

[5] Wan Dongdong, He Peng, Zhang Wu, et al. Fluid-structure coupling numerical simulation of carotid artery plaque. Journal of Medical Biomechanics, 38(1) (2022)78-84.

[6] Zheng Zhi, Geng Bo, Dong Junhong, et al. Numerical simulation of fluid-structure coupling between launching, ship and pier at different collision angles. Ship Mechanics, 27(4) (2023)15-24.

[7] Kong Xijun, XING Haojie, LI Hongjing. An explicit spectral element simulation method for fluid-structure coupling seismic wave problem. Chinese Journal of Theoretical and Applied Mechanics, 54(9) (2021)164-167.

[8] Wang Rongpeng, SONG Guiqiu, ZHOU Shihua. Dynamic simulation of fluid-structure coupled drill string system. Journal of Northeastern University: Natural Science Edition, 43(1) (2022)98-102.

[9] Wang Ping, Zhang Aman, Peng Yuxiang, et al. Study on meshless numerical simulation of transient strong nonlinear fluid-structure coupling in near-field underwater explosions. Chinese Journal of Theoretical and Applied Mechanics, 54(8) (2021)16-22.